Design of photonic bands for opal-based photonic crystals

J.F. Galisteo-López, F. García-Santamaría, D. Golmayo,
B.H. Juárez, C. López*, E. Palacios-Lidón

Instituto de Ciencia de Materiales de Madrid (CSIC), C/ Sor Juana Inés de la Cruz 3, 28049 Madrid, Spain

Abstract

To make a device from an opal—or otherwise—the photonic bands and the optical properties derived from them are needed. Knowing the effects of different parameters defining the opal geometry and different possible modifications of its structure are needed, too. An accurate definition of the device will be required to obtain a good performance. With this aim, the optics of light with a wavevector in the vicinity of the L point in the Brillouin zone and its coupling to bare opals band structure are presented. An important aspect is the transition from finite to infinite crystal and the study of size effects on the bands. It is possible to substantially alter the photonic band structure of an opal-based system, while maintaining the lattice structure, simply by growing layers of other materials with an appropriate refractive index. Here, it is shown how, by the growth of accurately controlled thin layers of silicon and germanium, and further processing, one can induce the opening of two complete photonic band gaps (PBGs) in an opal structure. Finally, the possibility to fabricate a simple device consisting in a planar waveguide will be shown. By means of a very simple and inexpensive procedure, engineered planar defects acting as microcavities have been realized. These can be viewed as a particular case of a much more general class of heterostructures that can be grown by combining opal vertical deposition and chemical vapour deposition of oxides. A further step is made by applying electron beam lithography to provide lateral definition and facilitate three-dimensional structuring.
© 2004 Published by Elsevier B.V.

Keywords: Photonic crystals; Three-dimensional; Finite size; Band engineering; Opals; E-beam lithography

1. Introduction

Photonic crystals (PCs) [1,2] are called the building blocks of future all-optical devices, due to the unusual way in which these structures interact with electromagnetic radiation. In order to tailor the shape of a photonic band structure, a good choice of the lattice symmetry is important. Unfortunately, self-assembly methods allow few variations, since face centred cubic (fcc) structures of touching spheres are often the usual result [3]. However, when it comes to band engineering, it must be taken into account that photonic bands not only depend on the underlying lattice, but on the primitive cell structure. So, accurate control of the materials composing an fcc crystal is a remaining tool for band engineering. The use of high refractive index

* Corresponding author. Tel.: +34 913349019;
fax: +34 913720623.
E-mail address: cefe@icmm.csic.es (C. López).

semiconductors severely affects band structure. Varying the topography would involve changes and, therefore, is another tool to be considered.

Prior to considering artificial opals [4] as part of any technological application, their optical properties must be well understood. Further, an appropriate strategy to modify these properties is needed since different applications will require different performances. Finally, the technology to construct opal-based devices must be developed, even though in some cases it may be borrowed from other disciplines. In this sense, an intense effort is being dedicated to the materials aspects of photonic crystals [5].

In this work, we present an approach to these tasks. By means of reflectivity measurements, we study the optical properties of these systems and determine the optimal size for which finite size effects may be ignored and a comparison with calculated energy bands [6] (defined for infinite crystals) can be carried out.

Infinite crystal behaviour assured the energy bands along high symmetry directions are experimentally probed by means of reflectivity measurements. We have studied the role of defects by doping artificial opals with spheres of different sizes and nature.

We then explore how the optical properties of artificial opals can be tailored by modifying the composition of the unit cell. This is the only route, due to the fact that the lattice is fixed to fcc by the growth process itself. Growth of semiconductor mono-layers or even multiple layers combining air, Si, silica, Ge, and GeO_2 will be presented. Using this method, it will be possible to modify the photonic properties of the opals. To achieve the results presented here, thin glass and polymer opals were prepared by vertical deposition [7] on silicon and glass substrates. We propose a way to develop 2D cavities in opal-based photonic crystals, as a first approach to construct optical devices which may find applications in fields such as opto-electronics. Similarly, we developed a technique to laterally define submicron structures in opal materials.

2. Lattice

For a given underlying lattice, very different photonic behaviours may appear. A glass slide, an opal, or an opal infilled in a very complicated manner, and then
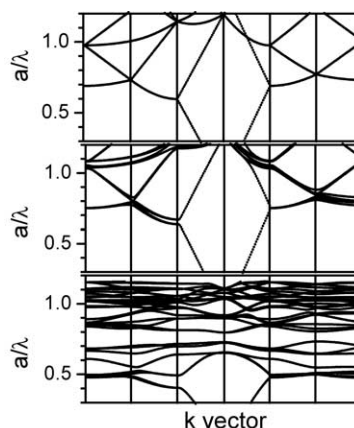
Fig. 1. Band structure for an fcc lattice with three different cell configurations: top: empty lattice (free photons); middle: bare opal; bottom: low Ge filling fraction inverted opal.

inverted, have the same lattice, but present optical properties ranging from free photon behaviour to multiple photonic band gaps (PBGs). This can be seen in Fig. 1, where the band diagrams for the mentioned structures are plotted in the energy range where the Bragg diffraction occurs. It can be seen that the gaps widen and the bands flatten as the refractive index contrast is increased. In particular, two complete PBGs can be opened in the last case, where an fcc lattice of air spheres with a high filling fraction is shown [8].

The main problem found in the preparation of artificial opals is the unavoidable presence of disorder generated by both the polidispersity of the micro-spheres used and the inherent stacking defects developed during the growth process.

It is well known that the presence of a defect in a PC, in analogy with the behaviour observed for electron crystals, introduces localized states within the energy gap in a well defined position [9]. If the defects are randomly distributed, the optical response is given by the average for all defect configurations, resulting in a decrease of the Bragg peak intensity [10]. One way of introducing structural disorder in artificial opals is by adding controlled amounts of dopant spheres of sizes different from those of the host. By using the vertical deposition method [7], polystryrene (PS)-doped poly-methyl-methacrylate (PMMA) samples are obtained. The maximum reflectance (at normal incidence) for frequencies contained in the
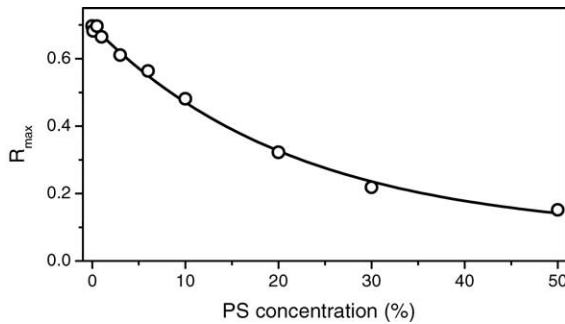
Fig. 2. Maximum reflectance from a 270 nm thin film PMMA opal as a function of doping concentrations (ranging from 0.01% to 50%) with 350 nm PS spheres. The line is an exponential decrease fit.

pseudogap for PMMA thin film opals of 270 nm spheres doped with different concentrations (from 0.01% to 50%) of 350 nm PS spheres is shown in Fig. 2. As expected, the Bragg peak intensity decreases as the PS spheres concentration increases in agreement with previous results reported by Gates and Xia [11]. This proves that the structural disorder in the PCs increases with the dopant concentration in the host matrix. Similarly, by increasing the size of the defect, while keeping its concentration constant, a worsening of the optical properties is attained [12].

Defects produce scattering and propagation becomes diffusive: Reflectance and transmittance do not add up to one. In the absence of absorption, diffuse scattering in this spectral region can be measured as the intensity being neither reflected nor transmitted: (1-R-T). As seen in Fig. 3, apart from a steady increase
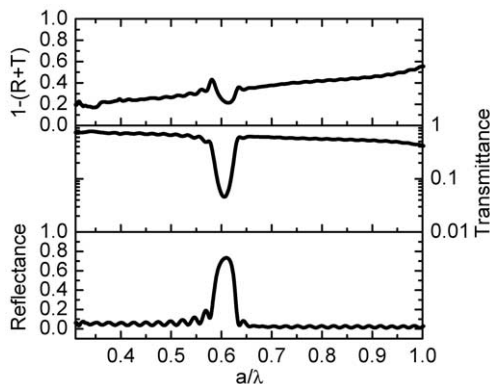
with frequency (Rayleigh scattering), diffuse intensity presents a maximum at the low energy edge of the gap and a minimum inside the gap. This effect increases with the size of the system (number of layers of the sample). The maximum occurring in the low energy edge of the gap can be explained as the momentum exchange, Δk, necessary to scatter into a propagating state from the edge of the band at the L point, which is smaller for energies closer to the lower edge than elsewhere [10].

3. Finite size effects

Photonic bands is a concept that belongs to crystals and entails a lattice infinite in three-dimensional space. For the samples under study, the dimensions perpendicular to the probing beam are on the order of one centimetre. However, in the direction parallel to the incident beam, the crystal will consist of just a few layers. It is important to determine how many layers are needed to consider our crystal infinite. The question arises on how to decide the crystal has achieved an infinite crystal behaviour. A number of parameters, which can be employed to characterize the reflectivity peak associated with the pseudogap at the L point in the Brillouin zone, such as its centre frequency or the edges, were considered in order to gain insight into the size effects present in the system. It was observed that the only parameter that could be used for this purpose is its full-width at half-maximum (FWHM) [13].

In Fig. 4, we present a comparison between theoretical predictions and experimental results. The horizontal line, indicating the infinite crystal pseudogap

Fig. 3. Reflectance (bottom) and transmittance (middle) do not add to one, the difference is diffuse scattering (top). This is most intense at the low energy edge of the gap.
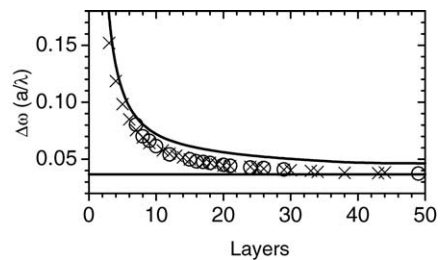
Fig. 4. Comparison between experimental (symbols) and calculated (lines) data. Experimental data from samples grown on silicon (○) and fused silica (×) are shown. Theoretical data extracted from scalar wave approximation for finite crystals (curve) and photonic band calculations for infinite crystal (horizontal line) appear.

width, was extracted from exact band structure calculations [6]. We can see that size dependence disappears for samples thicker than 35 layers. It was also observed [13] that the influence of size effects on some Bragg peak features (centre and edges) are different, depending on the substrate on which the sample is grown (not shown). Therefore, these parameters are not only dependent on the finiteness of the sample, but also on its optical environment. Thus, FWHM can be taken as representative of electromagnetic radiation interaction with the photonic crystal alone, and not its optical environment.

Here, we mention that the criterion used to consider our crystal as an infinite one is a first approximation to the study of finite size effects in artificial opals. In order to further investigate this subject, other magnitudes such as the density-of-states could be used [14].

4. Orientation

Provided the sample thickness for which the infinite crystal behaviour is reached, at least in the spectral region where first order Bragg diffraction takes place, we may carry out a comparison with calculated energy bands. The possibility of knowing a priori what the orientation of our samples is by means of optical diffraction [13] will allow us to probe the optical properties of the crystals along certain high symmetry directions.

Owing to the characteristics of the growth by the vertical deposition method, it is possible to select the scan in the hexagon around the L point. By rotating the sample around an axis parallel to the meniscus line, k is contained in the ΓLW plane. On the contrary, if the rotation axis is perpendicular to it and parallel to the meniscus displacement, k is contained in the ΓLU plane [13].

In Fig. 5, the reflectance peaks found along these two paths (ΓLU and ΓLW) are investigated by tilting the k_i off the normal to the sample. For the spectra presented in left (right), the incident and reflected wave vectors are contained in the ΓLU (ΓLW) plane in reciprocal space. Experimental results present avoided crossing behaviour [15,16] taking place at the U (W) point in reciprocal space. Here, the incident wave vector fulfills simultaneously the Bragg condition for one {1 1 1} and one {1 0 0} families of planes
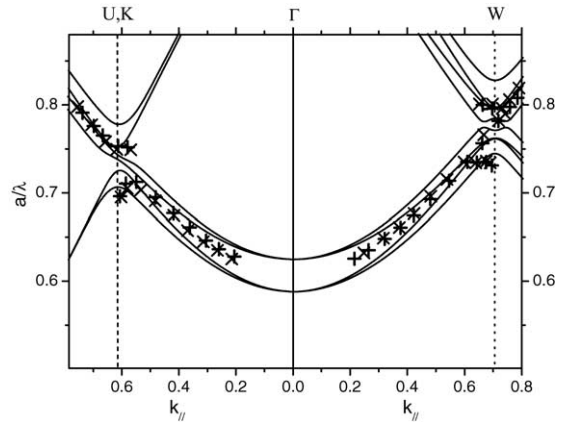
Fig. 5. Bragg peak dependence on angle with respect to the normal plotted in two directions: towards U and towards W points in reciprocal space. Experimental data (scattered symbols) are compared with photonic bands calculated along the L → U direction (left) and L → W (right).

(U), or for two {1 1 1} and one {1 0 0} planes (W). The two sets of data plotted for each direction are obtained by rotating the sample 60° around its normal. Coincidence of both sets is expected, since the K and U points are equivalent in artificial opals [17].

5. High energy bands

Attention has so far been concentrated on the Bragg peak and very few studies have been devoted to the high energy regions [18]. Reflectance and transmittance in the mentioned spectral range present a rich structure [19] as can be seen in Fig. 6. This corresponds to an abrupt change in the band structure of the crystal, which turns from the linear behaviour found in the surrounding of the pseudogap to a complicated bundle of bands. We can divide the energy bands into those which come from wave-vectors, k, parallel to the incident direction (thick lines in Fig. 6) and those coming from k's originally not parallel to that direction, but folded back to it by translational symmetry (thin lines) [20]. After doing so, we can see in Fig. 6 how the features in reflectance (peaks) and transmittance (dips) spectra may be correlated to perturbations of the former set of bands. These perturbations may take place as splitting at the edges and centre of the Brillouin zone or band anticrossings. For reduced frequencies around $a/\lambda = 1.15$, close to where second
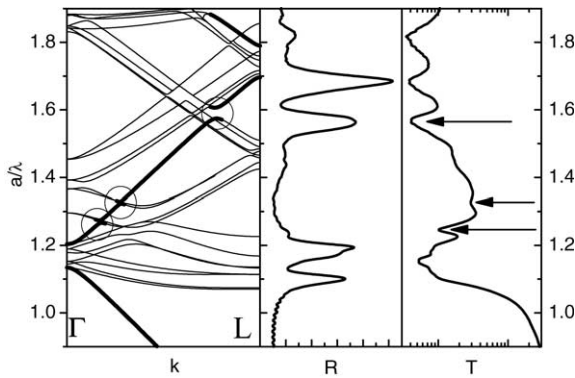
Fig. 6. Calculated band structure (left), and experimental reflectance (middle), and transmittance (right) for a PS opal having 35% of the pore filled with SiO_2.

order diffraction by the {1 1 1} planes would be expected, if no other planes were considered, we see two peaks in reflectance (for $a/\lambda = 1.1$ and 1.2) which coincide with a broad dip in transmission. The nature of these peaks is clearly different from that of the pseudogap ($a/\lambda = 0.6$), since, in the latter, the peak was due to the lack of available states. Here, a number of bands presenting a very low slope are present, so that light may couple to them. Energy bands presenting a low slope have been theoretically predicted to behave as an effective medium with a high refractive index, and, therefore, a high (low) reflectance (transmittance) could be expected.

Similar features may be found for higher frequencies. Anticrossings at $a/\lambda = 1.27$, 1.33, and 1.59 are accompanied by dips in transmission (pointed by arrows in the spectrum). Only the last one, spectrally the widest, may be seen in reflectance. Finally, at $a/\lambda = 1.7$ a reflectance peak and a transmission dip are found close to the value where third order Bragg diffraction would be expected in the scenario where only diffraction by the {1 1 1} planes is considered. Again, the nature of these features differs from that of the Pseudogap, since energy bands are present for these frequencies.

In summary, we can see that features in normal incidence reflectance and transmission spectroscopy are related to perturbations (such as splitting and anticrossing) of those bands originated by k's parallel to the incident direction. Further research is being carried out in order to investigate the exact role of energy bands in this energy region.

6. Infiltration with Si/Ge

Silicon and germanium can be synthesized by chemical vapour deposition (CVD), performing slight modifications over already published methods [21,22]. With a fine control over Si and Ge synthesis, the growth of multilayer structures can be achieved. This method allows growing both materials on silica and either on the other. In a typical procedure, the sample is placed in a cell where the precursor gas is condensed with liquid nitrogen. The precursor gases used in this work were disilane (Si_2H_6) for Si and germane (GeH_4) for Ge. In the case of Si, the precursor gas decomposition temperature selected was 375 °C, while for germane it was set at 270 °C. Lower temperatures resulted in very slow synthesis rates, while higher ones allowed low quality and growth control. The result is the growth of a thin layer of semiconductor covering the surface of every sphere in the opal and precisely replicating the template. For a given amount of precursor in the reactor (that can be characterized by the pressure), the amount of semiconductor deposited in the sample can be very accurately controlled by the reaction time (at the selected temperature) and precisely monitored through the optical properties [8].

A further degree of freedom is provided by the selectivity of different solvents that can be used to remove some of the materials. Diluted HF can be used to remove silica with no effect on Si or Ge. *Aqua regia* (a mixture of hydrochloric and nitric acid) can selectively remove Ge, not damaging silica nor Si. Furthermore, Ge can be oxidized at 500 °C without altering the properties of the other materials.

A test of the possibilities of the method is proposed in Fig. 7. After loading an opal with a layer of Si, a layer of Ge is added; finally, a second Si layer fills the pores to 60%. This sample is then dipped in *aqua regia* for 60 min. The outcome is two homogeneous Si shells separated by an air gap, the inner shell being connected to the silica spheres. The process is shown in the lower sequence in Fig. 7 and the corresponding optical spectra are plotted in Fig. 8. The bare opal (a) is loaded with Si (b). The first pseudogap all but disappears while higher energy features become clearer. Further loading with Ge (c) raises the first pseudogap and increases reflectance peaks width. A new layer of Si (d) further red-shifts and widens photonic features. At this point, Ge begins to become etched. Before it is
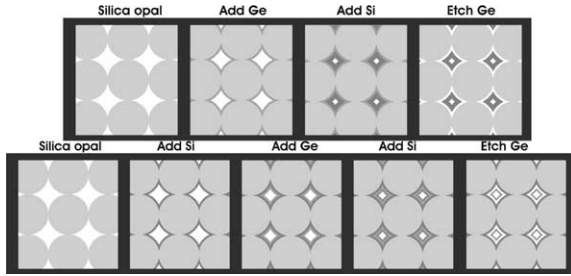
Fig. 7. Diagram showing two strategies for the formation of multi-layer systems. The upper row shows the formation of an opal surrounded by a Si layer with an air gap between the spheres and the Si layer. The lower route proposes the way to form a double layer of Si separated from the echo by an air gap with the innermost Si layer touching the spheres. Its optical monitoring is shown in Fig. 8.

Fig. 8. Reflectance spectra of a sample as semiconductors infilling and etching proceed. (a) Bare opal; (b) Si layer grown; (c) second layer: Ge and (d) third layer: Si; (e) partial etching of Ge; (f) etching is completed.

completely removed, spectra were collected from areas with and without Ge at the same time. Both diffraction peaks corresponding to the first pseudogap of each case appear in the spectrum at 2.22 and 1.85 μm, respectively (e). After the etching was completed in 60 min (f), the peak at 2.22 μm has completely disappeared.

7. Band structure engineering

Although limited by the fact that symmetries other than fcc are very difficult to obtain, self-assembly giving rise to fcc lattices, engineering the photonic

band structure is still possible. Indeed, subtle variations in topography or refractive index contrast may lead to very interesting band structures. Here, the joint effects of air sphere interpenetration and incomplete semiconductor (Ge in this case) loading are taken into account. This four-step process illustrates a particular case where the multilayer technique described in the previous section may be applied to tailor the photonic bands. First, an opal is loaded with Ge to 25% of the available volume, followed by its oxidation. A further Ge load completes 86% of the initially available volume. Finally, the oxides (GeO_2 and SiO_2) are removed with HF. The corresponding photonic band structure is shown in Fig. 9. Two PBGs open now: a
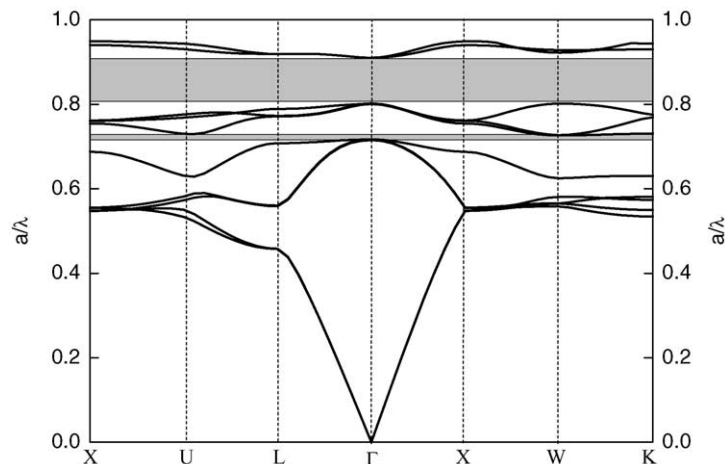
Fig. 9. Photonic band diagram of air spheres in a fcc lattice coated with Ge ($n = 4.1$). The radius of the air spheres is $0.3645a$ and the external radius of the semiconductor shell is $0.4087a$.

larger one (12.6%) between the 8th and 9th bands and a narrower one (1.3%) between the 5th and the 6th bands. The latter is an interesting case that only very recently has been reported for fcc-based structures [23]. The method could be simplified if SiO_2 CVD was used instead of growing Ge and then oxidizing it.

8. Vertical engineering

Using CVD, it is possible to engineer planar defects inside a photonic crystal by creating a heterostructure made of two slabs of SiO_2-infiltrated PS opal with the same sphere size, separated by a silica sheet of desired uniform thickness [24]. These types of structures, an example of vertical engineering, may find application as waveguides or lasers, and are obtained by sequential growth of thin film opals and silica slabs. The growth of the silica thin film planarizes the underlying opal and allows for further processing. Many different structures can thus be grown for different purposes. In this system, the lattice periodicity is broken by inserting a homogeneous sheet of a material with a refractive index lower than that of the composite opal. The position of the associated localized mode is expected to behave as an acceptor mode [9].

The reflectance of planar defects of silica film of varying thickness placed between two SiO_2/PS opals of 311 nm sphere size is shown in Fig. 10. A sharp resonance in the Bragg peak associated with the defect state is visible both in transmittance (not shown) and reflectance spectra at the same spectral position. Similar planar defects constituted by a layer of beads having a different diameter were also reported [25]. By changing the film's thickness, the dependence of the spectral position on defect size can be studied. The thickness of the SiO_2 film is controlled through the number of growth cycles used and checked by SEM inspection. The reflectance spectra (Fig. 10) show that the expected resonance appears at the conduction band edge and drifts across the photonic gap (Bragg peak) towards lower energy as the defect thickness increases. When the silica film reaches approximately the size of the opal spheres, the spectral position is at the valence band edge. If the thickness of the silica film is larger than the sphere size, the resonance re-enters the gap from the higher energy side and the process starts again [24].

We can now consider a similar structure, only that with inverted structures at both sides of the defect layer. When operating at wavelengths below the low frequency edge of the pseudogap, the inverse opals confining the cavity behave as a medium with an effective refractive index smaller than that of pure silica, which constitutes the guide, thus allowing total internal reflection. By changing the material constituting the inverse opals, which confines the planar defect for materials having larger refractive indices (i.e., Si or Ge) and would open a full PBG, the quality factor of the cavity could be enhanced allowing for a better confinement of the photons at the defect. This would improve the performance of the structures both, as a cavity for laser action and as a planar wave guide, in which light guiding would take place by Bragg diffraction for frequencies within the PBG.

9. Lateral engineering

Thin PMMA artificial opals were infiltrated with SiO_2 by CVD. Patterning of the PMMA/SiO_2 composite can be performed by e-beam lithography (EBL) thanks to the transparency of thin silica to the e-beam. Since PMMA presents a photo resist effect, it can be exposed and developed (in methyl isobutyl ketone), and the exposed areas subsequently dissolved. After developing the exposed areas, selective inverted opals were obtained [26]. The method is very convenient in order to introduce controlled three-dimensional
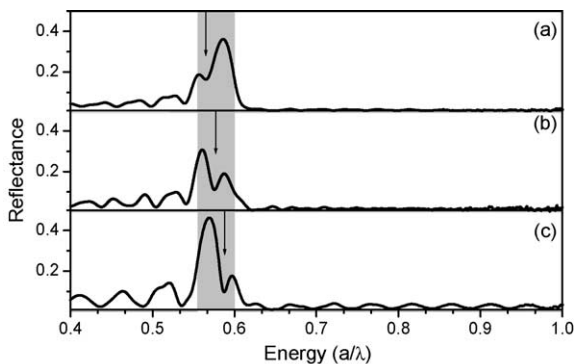
Fig. 10. Reflectance spectra of engineered defects in 311 nm SiO_2/PS opals. Silica films of: (a) 280 nm; (b) 230 nm; and (c) 130 nm embedded in the photonic crystal.
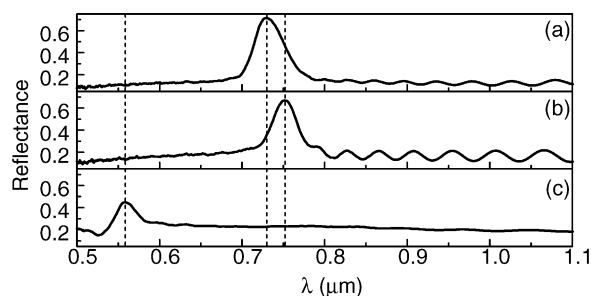
Fig. 11. Reflectance from: (a) bare PMMA opal; (b) PMMA/SiO$_2$ composite; and (c) exposed, developed, and inverted opal.

defects in 3D photonic colloidal crystals. Because of its potential application in creating structures for guiding and confinement of light, the method may find uses in the field of integrated optoelectronic circuits. In addition, the resulting channels, combining micro and nano features, may be very useful in the construction of microfuidic architectures for bionano-technology purposes.

Different patterns were obtained at an accelerating voltage of 25 kV and doses ranging from 100 to 850 μC/cm^2. The higher doses (in excess of 300 μC/cm^2) revealed effective for patterning the whole thickness of the opal (around 24 layers and sphere diameter 330 nm). It is worth noting that although the drawn structures are clearly seen by optical means, they are hardly discernible by SEM, meaning that the surface morphology of the system is not affected.

Fig. 11a and b show the reflectance spectrum from a bare PMMA opal and the red-shifted spectrum for the PMMA/SiO$_2$ composite after the CVD process. Fig. 11c shows the experimental reflectance of the opal after exposure and subsequent development.

These selectively inverted structures allow further growth and processing, leading to 3D buried structures. The approach has genuine potential because it allows a posteriori control of a self-assembled structure. The relevance of the technique for the fabrication of integrated 3D architectures has been suggested.

10. Conclusions

We have presented a digest of some optical properties of artificial opals comprising finite size effects,

angle resolved measurements, and effects of disorder. Then, we modified the optical properties of our samples by modifying the morphology of the unit cell, which demonstrates that even with a fixed underlying lattice there is room for tuning the optical properties of self-assembled structures. Finally, experimental evidence of localized states in the pseudogap of artificial opals, introduced by means of 2D cavities, and examples of lateral texturizing of planar structures are presented.

References

[1] E. Yablonovitch, Phys. Rev. Lett. 58 (1987) 2085.
[2] S. John, Phys. Rev. Lett. 58 (1987) 2486.
[3] F. García-Santamaría, H.T. Miyazaki, A. Urquía, M. Ibisate, M. Belmonte, N. Shinya, F. Meseguer, C. López, Adv. Mater. 14 (2002) 1144.
[4] V.N. Astratov, V.N. Bogomolov, A.A. Kaplyanskii, A.V. Prokofiev, L.A. Samoilovich, S.M. Samoilovich, Y.A. Vlasov, Nuovo Cimento. 17 (1995) 1349.
[5] C. López, Adv. Mater. 15 (2003) 1679.
[6] S.G. Johnson, J.D. Joannopoulos, The eigenstates are computed using an iterative implementation of a plane expansion as in, Opt. Express 8 (2001) 173.
[7] P. Jiang, J.F. Bertone, K.S. Hwang, V.L. Colvin, Chem. Mater. 11 (1999) 2132.
[8] F. García-Santamaría, M. Ibisate, I. Rodríguez, F. Meseguer, C. López, Adv. Mater. 15 (2003) 788.
[9] E. Yablonovitch, T.J. Gmitter, R.D. Meade, A.M. Rappe, K.D. Brommer, J.D. Joannopoulos, Phys. Rev. Lett. 67 (1991) 3380.
[10] M.A. Kaliteevski, J. Manzanares-Martinez, D. Cassagne, J.P. Albert, Phys. Rev. B. 66 (2002) 113101.
[11] B. Gates, Y. Xia, Appl. Phys Lett. 78 (2001) 3178.
[12] B.H. Juárez, E. Palacios-Lidón, E. Castillo, C. López, SPIE Proc. (in press).
[13] J.F. Galisteo-López, E. Palacios-Lidón, E. Castillo-Martínez, C. López, Phys. Rev. B 68 (2003) 115109.
[14] D. Felbacq, R. Smaâli, Phys. Rev. B 67 (2003) 85105.
[15] H.M. van Driel, W.L. Vos, Phys. Rev. B 62 (2000) 9872.
[16] S.G. Romanov, T. Maka, C.M. Sotomayor Torres, M. Muller, R. Zentel, D. Cassagne, J. Manzanares-Martinez, C. Jouanin, Phys. Rev. E 63 (2002) 56603.
[17] J.F. Galisteo-López, F. López-Tejeira, S. Rubio, J. Sánchez-Dehesa, C. López, Appl. Phys. Lett. 82 (2003) 4068.
[18] H. Míguez, V. Kitaev, G.A. Ozin, Appl. Phys. Lett. 84 (2004) 1239.
[19] J.F. Galisteo-López, C. López, Phys. Rev. B 70 (2004) 035108.
[20] K. Sakoda, Optical Properties of Photonic Crystals, Springer-Verlag, Berlin, 2001.
[21] A. Blanco, E. Chomski, S. Grabtchak, M. Ibisate, S. John, S.W. Leonard, C. López, F. Meseguer, H. Míguez, J.P. Mondía,

G.A. Ozin, O. Toader, H.M. van Driel, Nature 405 (2000) 437.

[22] H. Míguez, E. Chomski, F. García-Santamaría, M. Ibisate, S. John, C. López, F. Meseguer, J.P. Mondía, G.A. Ozin, O. Toader, H.M. van Driel, Adv. Mater. 13 (2001) 1634.

[23] W.T. Dong, H. Bongard, B. Tesche, F. Marlow, Adv. Mater. 14 (2002) 1457.

[24] E. Palacios, J.F. Galisteo, B.H. Juárez, C. López, Adv. Mater. 16 (2004) 341.

[25] K. Wostyn, Y. Zhao, G. de Schaetzen, L. Hellemans, N. Matsuda, K. Clays, A. Persoons, Langmuir 19 (2003) 4465.

[26] B.H. Juárez, D. Golmayo, P.A. Postigo, C. López, Adv. Mater. (in press).